JOURNAL OF MATERIALS SCIENCE 24 (1989) 1273–1280

# X-ray reflection topographic study of growth defect and microindentation strain fields in an RDX explosive crystal

W. L. ELBAN*, R. W. ARMSTRONG‡
*Naval Surface Warfare Center, Silver Spring, Maryland 20903-5000, USA*
K. C. YOO§, R. G. ROSEMEIER¶
*University of Maryland, College Park, Maryland 20742, USA*
R. Y. YEE
*Naval Weapons Center, China Lake, California 93550, USA*

A reasonably perfect cyclotrimethylenetrinitramine (RDX) explosive crystal has been studied by surface reflection (Berg–Barrett) X-ray topography for the purpose of further elucidating the microstructural basis for hot spots forming in secondary explosives. Topographs were obtained through the base $(\bar{2}\,1\,0)$ surface of a crystal grown by slow evaporation from an acetone solution. $(\bar{7}\,2\,\bar{1})$ and $(\bar{6}\,3\,\bar{2})$ reflections have revealed the central strain field of a large growth defect. This type of defect is proposed to be a suitable internal obstacle for triggering dislocation pile-up collapse during crystal deformation and fracture. Also, extremely localized plastic deformation zones were revealed at Knoop microindentations employed to measure the hardness anisotropy in the $(\bar{2}\,1\,0)$ crystal surface. A combination of restricted slip systems and cracking is responsible for the significant anisotropy.

## 1. Introduction

Historically, the sensitivity of crystalline explosives, determined by drop-weight impact testing, has been assessed on the basis of chemical factors. Considerable insight has been gained from this approach. For example, the 50% initiation impact heights for various organic high explosives have been related to their oxidant balance values [1, 2]. However, explosives have important microstructural properties which are masked through the use of sandpaper placed on the anvil surface. Otherwise, the plastic deformation and cracking behaviour of explosives responding to impact loading are reasoned to be important considerations. Thus, it was concluded that the microstructural properties of explosives and their concomitant mechanical properties should be investigated. This would provide a more complete understanding of how mechanical work is concentrated locally and converted to hot spots as originally proposed by Bowden and Yoffe [3]. The contribution of hot spots to determining the impact sensitivity of explosives is of special interest.

One consequence of the foregoing considerations was the development of a dislocation pile-up model for the origin of hot spots within deforming materials [4–6]. A hot spot site was proposed to be triggered by the sudden collapse of individual dislocation (slip band) pile-ups blocked by internal obstacles. Considerable adiabatic heating was predicted to occur from the accumulated dislocation interaction energy dissipated by catastrophic pile-up collapse.

The conventional method of drop-weight impact testing of loose piles of explosive crystals provides a rather complicated measure of the combined mechanical properties of an explosive material. Alternatively, individual explosive crystals themselves are not typically of convenient size for most of the well-defined deformation experiments conventionally performed on other materials. Microhardness testing provides a reasonably controlled way of locally deforming crystals so as to obtain information on their active slip systems, the degree of plastic anisotropy, and the ease of cracking.

Previous results have been reported [7, 8] for the nature of plastic anisotropy in laboratory-grown cyclotrimethylenetrinitramine (RDX) explosive crystals. This was accomplished by placing 0.5 $N$ Knoop microindentations at various crystallographic orientations on several prominent natural growth facets. The crystals were a few millimetres in size and had been grown from solution in acetone by evaporation at room temperature. A considerable variation in Knoop microindentation hardness pressure, ranging from 170 to 700 $N\,mm^{-2}$, was measured. This

*Present address*: Department of Engineering Science, Loyola College, 4501 North Charles Street, Baltimore, Maryland 21210, USA.
† *Present address*: Department of Mechanical Engineering, University of Maryland, College Park, Maryland 20742, USA.
§ *Present address*: Westinghouse Electric Research and Development Center, Pittsburgh, Pennsylvania 15235, USA.
¶ *Present address*: Brimrose Corporation of America, 7720 Belair Road, Baltimore, Maryland 21236, USA.

0022–2461/89 $03.00 + .12 

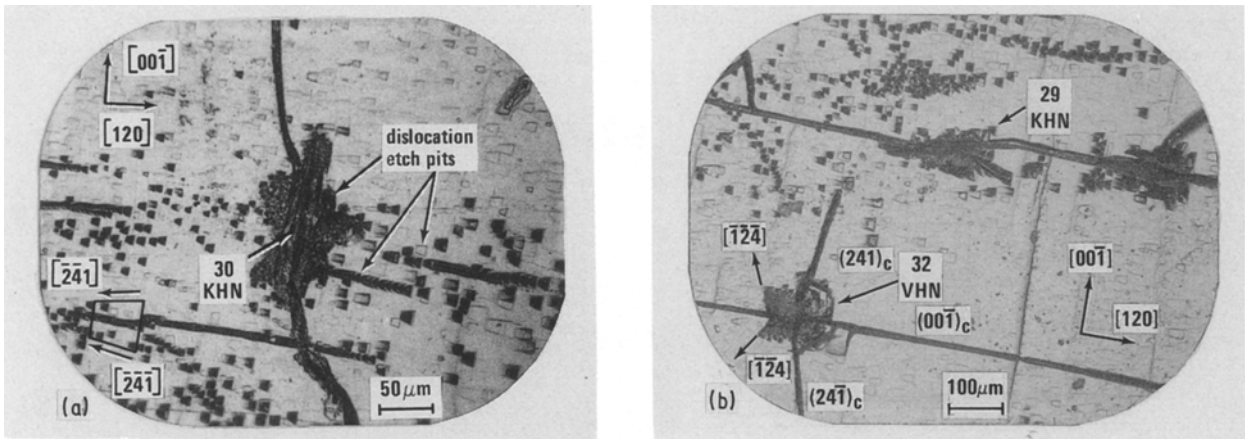


*Figure 1* Dislocation etch pits centred on microindentations in the ($\bar{2}$ 1 0) growth surface of RDX: (a) Knoop indentation nearly parallel to [0 0 $\bar{1}$]; (b) Vickers indentation with one diagonal parallel to [0 0 $\bar{1}$] (after Elban and Armstrong, [7]).

suggested that RDX has a limited number of operative slip systems and/or that considerable interference occurred between dislocations on the various systems. Extremely localized arrays of dislocation etch pits [9] were observed [7, 10] to be centred on the microindentations (Figs 1a, b). The surface area of the plastic zones was found to be only about 11 times greater than the projected area of the indentations, far less than observed, for example, for ionic crystals [7]. A considerable Knoop microindentation hardness anisotropy was also measured in a preliminary study of (Holston) production-grade Class D crystals of about 1 to 2 mm in size [8]. Similar observations have been made by Halfpenny *et al.* [11] in a more recent etch-pitting study of indented laboratory-grown RDX crystals.

An objective of the current work was to investigate the use of X-ray surface reflection (Berg–Barrett) topography for providing information on the microstructural properties of reasonably perfect RDX crystals. A relatively large crystal of approximately 0.5 cm$^3$ was grown by an acetone solution evaporation technique. Surface reflection topography observations were made of the initial crystal perfection and of the nature of the localized plastic deformation patterns at the Knoop microindentations.

## 2. Crystal growth and characterization

The starting material was doubly recrystallized Holston RDX. Care was taken to limit chemical degradation of the RDX that could occur either by exposure to light or elevated temperature. A stock solution of the doubly recrystallized material in distilled technical grade acetone was prepared. Excess RDX crystals were introduced to the solution which was stored, in a brown bottle, for a week at ambient temperature to allow for continued slow dissolution of the RDX. Next, the stock solution with excess RDX crystals, was put into a flask fitted with a heating mantle and a reflux condenser in order to prepare a hot saturated solution. The mixture was gently refluxed at about 56° C for 30 min.

Crystal growth was accomplished by adding 375 ml filtered hot saturated solution to 25 ml fresh acetone in a 500 ml Erlenmeyer flask. Four seed crystals were placed at different areas on the bottom of the flask, whose opening was then tightly covered with aluminium foil. The flask was stored at ambient temperature in an isolated dark area. Generally, more than four crystals were observed to grow to about 0.5 cm$^3$ in 5 to 7 days. To avoid cracking of the crystals, special precaution was taken to reduce any thermal stress generated as the crystals were removed from solution. The procedure was to decant all but 1 ml of the solution and then to position the flask so that no crystal was touched by any solution. The remaining solution was allowed to evaporate slowly.

A crystal resulting from this growth procedure is shown in Fig. 2a. The morphology of the crystal, as determined from a zone analysis of its Laue X-ray back-reflection pattern, was found to fit a new prismatic morphology described [7, 8] for some of the laboratory RDX crystals grown from acetone under less controlled conditions. Various growth surfaces and crystal directions are specified in Fig. 2b. The degree of microstructural perfection of this crystal appears to be significantly improved over crystals studied previously [7, 8], as evinced even by the gem-like optical transparence shown in Fig. 2a. Also, X-ray diffraction "spots" were sharp in the Laue photograph. Some streaking of a few spots was observed. The ledge structure which is visible in Fig. 2a is on the far crystal surfaces opposite to the specular ($\bar{2}$ 1 0) base surface through which the total crystal volume is being viewed. The terraced crystal facets have grown from the crystal base surface to give an overall thickness of the crystal of about 5 mm.

Considerable effort was devoted to microstructural characterization of the ($\bar{2}$ 1 0) base crystal facet by surface reflection (Berg–Barrett) topography [12–14]. Initially, two Knoop microhardness impressions were placed (Fig. 3) at 0.5 N load in the top portion of the ($\bar{2}$ 1 0) growth surface to serve as markers for detecting any variation in diffraction contract in the topographs. For both indentations, the long axis of the Knoop indentor was aligned parallel to [0 0 $\bar{1}$]. The ($\bar{2}$ 1 0) surface was positioned to fully support the indentor in only one case. A large crack resulted in the second instance of partially supporting the indentor across the [1 2 1] direction at the ($\bar{2}$ 1 0)–($\bar{1}$ 1 $\bar{1}$) edge of the crystal (Fig. 2b).

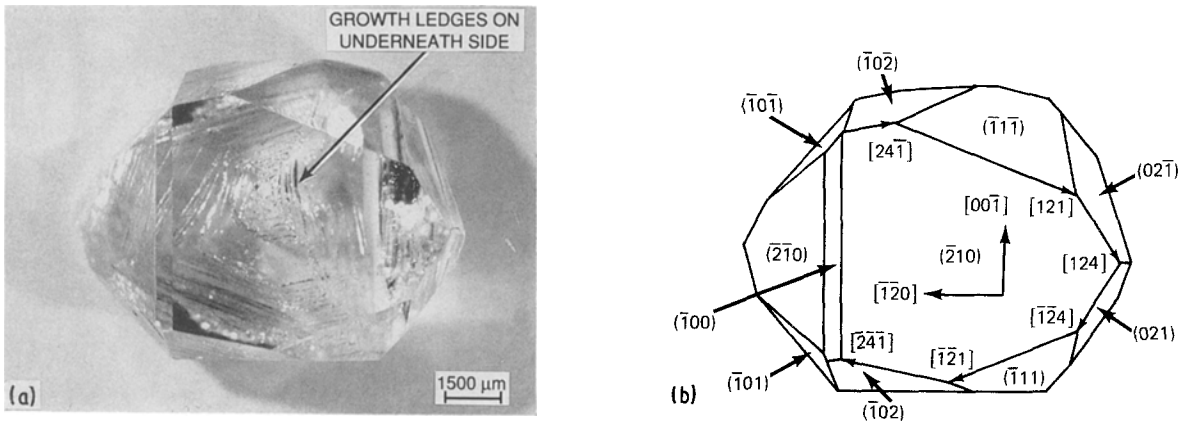


*Figure 2* Laboratory-grown RDX crystal: (a) light (Zeiss Tessovar) photograph; (b) schematic drawing identifying growth surfaces and directions.

A $(\bar{7}\,2\,\bar{1})$ surface reflection (Berg–Barrett) topograph obtained with Cu$K\alpha$ radiation, of a portion of the initially indented RDX crystal is shown in Fig. 4a. By reference to Fig. 3, the diffraction contrast at the two indentation positions is readily apparent. An enhanced diffracted intensity was presumed to occur at the indentations because of the lattice misorientation and/or cumulative residual dislocation strain fields associated with cracking at the residual microhardness impression. Of equal prominence in Fig. 4a is a totally different source of diffraction contrast near to the centre of the diffraction pattern. This source of diffraction contrast has been labelled "growth strain centre" in the $(\bar{6}\,3\,\bar{2})$ reflection of Fig. 4b. An improvement in resolution of the X-ray topograph was achieved for Fig. 4b by reducing the specimen-to-film distance from 10 mm for Fig. 4a to 4 mm for Fig. 4b. The problem of overlapping images in the various crystal positions prevented the obtaining of a smaller specimen-to-film distance. A stereographic description [14, 15] of the surface reflection (Berg–Barrett) topography alignments is given in Fig. 5. The two crystal positions are rotated approximately 80° to one another about the normal to the $(\bar{2}\,1\,0)$ surface. Fig. 5 is rotated 90° counterclockwise relative to Fig. 2b.

## 3. Knoop microindentation testing

Using a Tukon microhardness tester (Model FB), further Knoop hardness testing (0.5 N load) was performed on the $(\bar{2}\,1\,0)$ growth surface in regions away from the large growth strain centre in order to assess the degree of plastic anisotropy. The long axis of the Knoop indentor was aligned nearly parallel to the $[0\,0\,\bar{1}]$ and at a number of roughly 15° intervals counter-clockwise from that direction. In addition, alignment was also made with a few crystallographically prominent directions that were the intersection of other growth facets with the $(\bar{2}\,1\,0)$ surface. Care was taken to maintain orthogonality between the applied force axis of the indentor and the $(\bar{2}\,1\,0)$ growth surface. The crystal was affixed to a four-point stage using double-sided tape and levelled before each indentation was made. The use of the tape results in measured hardness values being a little lower than actual values.

The hardness anisotropy for the $(\bar{2}\,1\,0)$ growth surface is shown in Fig. 6. Included with the current measurements are previous values obtained [7, 8] for this same type of growth surface exhibited by another laboratory-grown crystal. The maximum Knoop hardness occurred for the indentor axis aligned near to the $[\bar{1}\,\bar{2}\,\bar{4}]$. Some cracking occurred around all of the

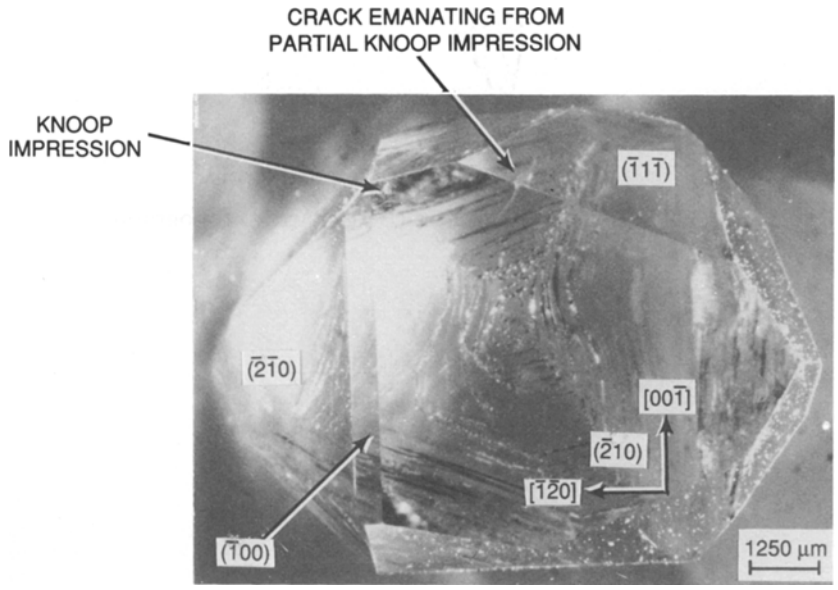


*Figure 3* Laboratory-grown RDX crystal with initial two Knoop indentations.

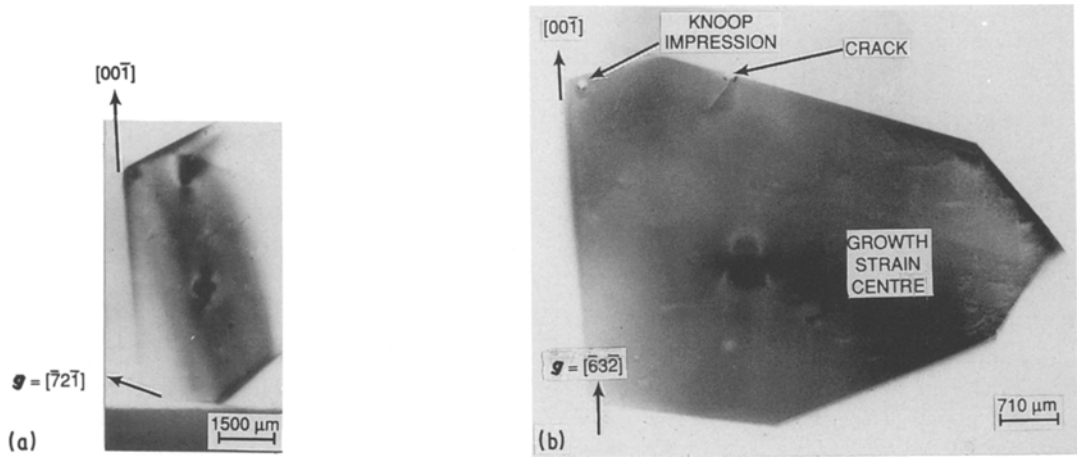


*Figure 4* Surface reflection (Berg–Barrett) X-ray topographs obtained prior to extensive Knoop hardness testing: (a) $(\bar{7}2\bar{1})$ reflection (b) $(\bar{6}3\bar{2})$ reflection. Cu$K\alpha$ radiation at 14 KV and 20 mA for (a) 3 h, and (b) ~2 h, on Ilford L4 50 $\mu$m nuclear plate.

indentations. Significant cracking and correspondingly lower hardness values resulted when the indentor was aligned along the $[\bar{2}\,\bar{4}\,\bar{1}]$ and $[0\,0\,\bar{1}]$ directions. Overall, reasonable consistency is shown between the two sets of measurements, although the microstructural perfection of the crystal used in the current work was judged to be superior. A larger degree of anisotropy was measured in the earlier work.

## 4. Knoop indentation strain fields

The strain fields of the Knoop indentations are shown in the $(\bar{6}\,3\,\bar{2})$ reflection topographic image in Fig. 7. The absence of any diffracted intensity at the white zones in the immediate vicinity of the actual indentation sites is the result of the material there not satisfying the Bragg condition. Adjacent to these zero diffracted intensity zones are narrow black regions of enhanced diffracted intensity. This indicates that the dislocations involved in forming the residual hardness impressions are highly concentrated in the vicinity of the indentation sites. The highly localized strain fields, observed by X-ray reflection topography, confirm the previous results obtained from dislocation etch pit studies [7, 11].

## 5. Discussion

### 5.1. Crystal growth

The crystal morphology observed in Figs 2 and 3 was identified as a new RDX growth form by Elban and Armstrong [7]. The chemical etch pit results shown in Fig. 1 were obtained on the $(\bar{2}\,1\,0)$ surface of an RDX crystal studied previously [7]. This crystal exhibited a relatively greater length normal to the $(\bar{2}\,1\,0)$ and a relatively reduced thickness along [1 0 0]. Some repetition occurs for particular directions and planes which are involved in either the crystal growth morphology, the shapes of etch pits or the etch-pitted deformation patterns centred on the micro-indentations. For example, the $[2\,4\,\bar{1}]$ direction, which defines the normal shape of a dislocation etch pit in

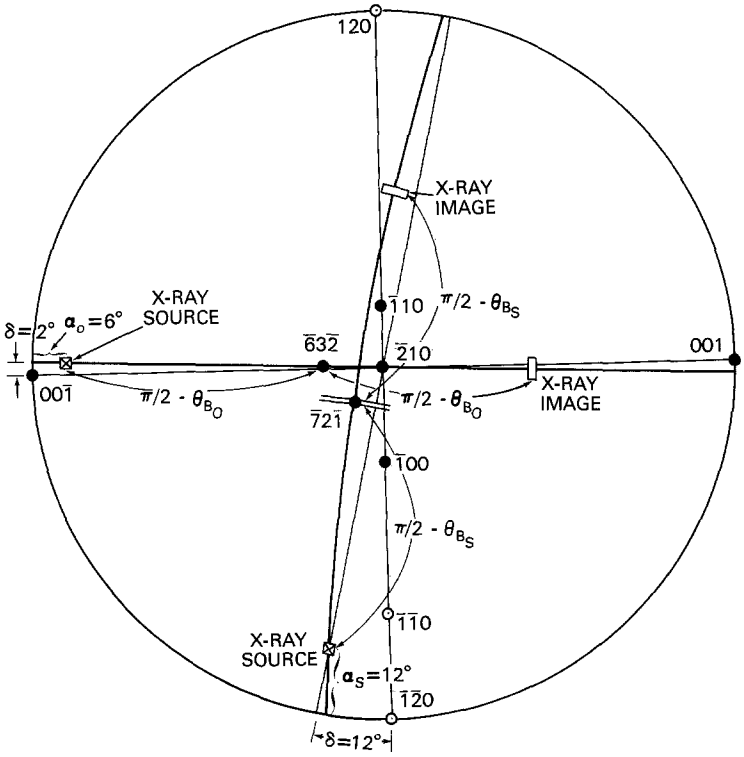


*Figure 5* $(\bar{2}\,1\,0)$ stereographic projection for X-ray topography alignment to study RDX. (●) plane normal, (○) plane direction.

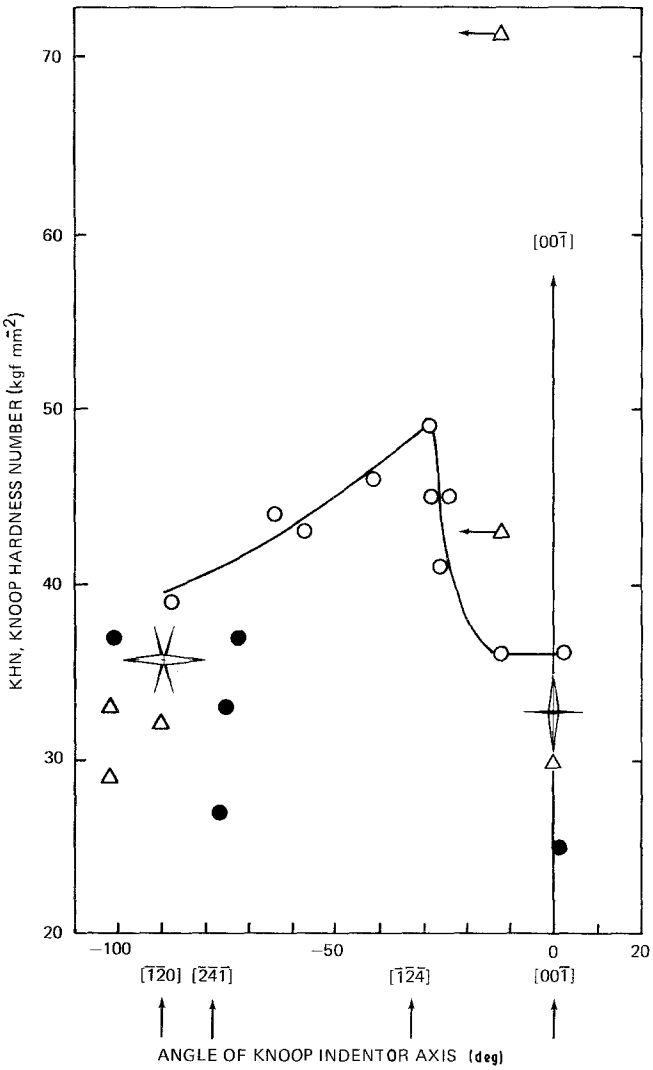


*Figure 6* Knoop hardness anisotropy for laboratory-grown RDX crystals (after Armstrong and Elban [10]). ($\bar{2}$ 1 0) RDX growth surface: (○) NWC crystal, (●) significant cracking; (△) NSWC crystal. Calibration test block measurements: 101 KHN, 100 ± 1.7 KHN.

Fig. 1a, is a crystal growth edge between the prominent ($\bar{2}$ 1 0) surface and the ($\bar{1}$ 0 $\bar{2}$) side face of lesser area (Fig. 2b). The [$\bar{1}$ $\bar{2}$ $\bar{4}$] direction for the slip band trace of etch pits in Fig. 1b was employed to define the (0 2 $\bar{1}$) slip plane which is shown to produce the same direction edge with the ($\bar{2}$ 1 0) surface in Fig. 2b.

The X-ray revealed strain centre in Figs 4a and b was imaged through the mirror-like front ($\bar{2}$ 1 0) surface opposite to the back (2 $\bar{1}$ 0) on which the crystal was mounted. The terrace and ledge structure on the opposite (2 $\bar{1}$ 0) surface is clearly observed through the total crystal thickness of approximately 5 mm. Presumably, the terrace and ledge structure was produced by spreading dislocation bundles emanating from the central crystal seed and penetrating the main (2 $\bar{1}$ 0) growth face associated with crystal thickening. Klapper [16] has described the importance of this occurring on a minimum dislocation line energy basis. McDermott and Phakey [17] have reported Lang transmission topographic observations of dislocation bundles penetrating {1 1 1} growth sector surfaces of prismatic crystals produced by slow growth from saturated solutions of RDX in dimethyl formamide (DMF). Halfpenny *et al.* [18] reported the characteristics of dislocation growth families intersecting both {1 1 1} and {2 1 0} growth sectors for prismatic crystals obtained from saturated acetone solution. In addition to non-ledge associated pure [0 0 1] edge dislocations aligned along the normal to the {2 1 0}, these authors reported [1 0 0] Burgers vectors for inclusion-initiated dislocations with irregular line directions propagating close to normal to {2 1 0} for most of their lengths. Such dislocations could produce (0 1 0) slip if their line vectors deviated a minimum angle of approximately 30° from the ($\bar{2}$ 1 0) normal. These dislocations and additional irregular ones with ⟨1 1 0⟩ Burgers vectors are capable of producing the ledge structures observed

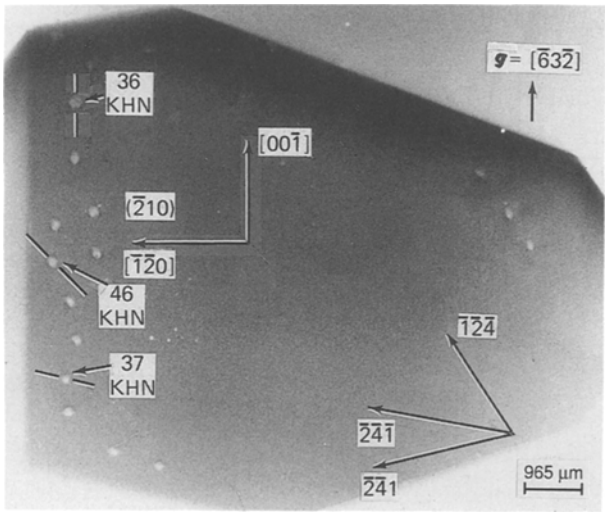


*Figure 7* Surface reflection (Berg–Barrett) X-ray topograph showing Knoop indentation strain fields. Cu$K\alpha$ radiation at 14 KV and 20 mA for 5 1/2 h on Ilford L4 25 $\mu$m nuclear plate.

for the $(2\,\bar{1}\,0)$ plane of the RDX crystal studied in this work.

Of significant interest is the possibility that few dislocation bundles are penetrating $(\bar{2}\,1\,0)$, through which the macroscopic strain field of the seed-like defect is observed. Little evidence of grown-in dislocations was observed in the X-ray topographs in Figs 4a and b. This is so, despite the indication from an assessment of the X-ray diffraction parameters (to be described later) that the surface reflection topographs should give relatively sensitive contrast of slight misorientation changes in the RDX lattice. Rather, the X-ray diffraction contrast observed for the strain field of the presumed seed-like defect is reminiscent of electron microscope observations of coherency strains at inclusions and precipitates, as described by Ashby and Brown [19]. Recently, Jung and Lefeld-Sosnowska [20] have detected, through transmission X-ray topography measurements, the presence of otherwise undetected local defects in silicon after subjecting crystals to a pressurizing treatment. This result was also related to the earlier work of Ashby and Brown. This consideration leads to the possibility that any plastic straining associated with the supposed seed crystal might be very localized near to the interfacial region. As such, the long-range stress field associated with the mismatch between the seed and newly grown crystal would be relatively ineffectively relieved. As mentioned earlier, a main result of previous etch pit results obtained at microindentations was that plastic flow in RDX is extremely localized in the immediate vicinity of the residual impressions.

## 5.2. X-ray topography

For a perfect RDX crystal placed in the surface reflection (Berg–Barrett) geometry, a very small angular width for the total reflection of X-rays satisfying the Bragg condition was calculated theoretically from the relationship [14, 21]

$$\Delta\theta_R = 2\lambda|\sin(\theta_B - \chi)|/\xi \sin 2\theta_B \qquad (1)$$

where $\lambda$ is the Cu$K\alpha$ wavelength of 0.154 nm, $(\theta_B - \chi)$ is the sum of the Bragg angle and (negative) angle between the $(\bar{6}\,3\,\bar{2})$ diffracting plane and the $(\bar{2}\,1\,0)$ crystal surface (Fig. 5), and $\xi$ is the dynamical extinction distance. For asymmetrical reflection, $\xi$ is given by

$$\xi = \left(\frac{mc^2}{e^2}\right)\frac{\pi V}{c\lambda|F|}\left[|\sin(\theta_B - \chi)|\sin(\theta_B + \chi)\right]^{1/2} \qquad (2)$$

where $(mc^2/e^2)^{-1} = 2.82 \times 10^{-13}$ cm, $V$ is the cell volume, $c$ is the (average) polarization, and $F(h\,k\,l)$ is the structure factor. A value of $\xi = 95\,\mu$m was computed to give $\Delta\theta_R = 4.1 \times 10^{-7}$ rad (0.000 023°). The value of $\xi$ compares favourably with the extinction distance of 120 $\mu$m computed for the (2 2 0) reflection obtained in transmission by McDermott and Phakey [17].

The requirement of using the higher order $(\bar{6}\,3\,\bar{2})$ and $(\bar{7}\,2\,\bar{1})$ surface reflections to minimize the influence of the geometrical divergence of the X-ray beam on image resolution has had the effect of giving a narrower reflecting width for total reflection of X-rays and, also, relatively reduced diffracted intensities. On this basis, the strain field of the major growth centre has been mainly revealed due to the changed orientation of the surrounding lattice planes over macroscopic distances within the crystal. The defect contrast appears analogous to that observed in very nearly perfect crystals studied by double-crystal monochromatic topography techniques [14].

As indicated earlier, the "double-lobed" pattern of diffraction contrast appears geometrically similar to that observed in other studies by transmission electron microscopy of precipitate particle strain fields, extending over distances orders of magnitude smaller. Alternatively, the residual deformation strains at hardness microindentations have been observed in topographs, in general, to be extremely localized at the edges of the indentations or at the tips of cracks spreading from the impression sites. The diffraction contrast at the indentations appears to be due largely to the reduction of primary extinction of X-rays by the cumulative strain fields of the dislocations. The dislocation contrast has been very nearly optimized more recently in a $(\bar{1}\,0\,0\,0)$ topograph of microindentations put into an RDX crystal obtained from H. H. Cady at the Los Alamos National Laboratory. The observation of extremely localized contrast suggests that the dislocations are arranged in an effective dipole geometry. This dislocation arrangement would be facilitated by internal (hot spot) heating and by the high homologous temperature ($T/T_M$ is 0.625, where the melting temperature, $T_M$, for RDX is 477 K) at which the hardness experiments on RDX were conducted.

## 5.3. Microindentation hardness anisotropy

The Knoop hardness anisotropy measurements appearing in Fig. 6 revealed that significant cracking resulted for two indentor alignments. Very visible cracking on the $(0\,0\,\bar{1})$ plane occurred when the long indentor axis was oriented near [0 0 1]. When the indentor was positioned near to the orthogonal $[\bar{1}\,\bar{2}\,0]$ direction, significant cracking occurred on either the $(2\,4\,\bar{1})$ or (2 4 1) plane or both. Thus, the occurrence of prominent cracking has its own orientation dependence somewhat analogous to the consideration of an orientation dependence for slip which has traditionally been credited with explaining the microhardness anisotropy. In the Knoop hardness test, cracking is most favourable when the crack plane is parallel to the short axis of the indentor, or nearly so. The wedge-opening strain between adjacent facets is greatest at this position on the indentor perimeter. The $(2\,4\,\bar{1})$ and (2 4 1) cracking systems for the [1 2 0] alignment have not been previously reported. Prominent cracking for the $[0\,0\,\bar{1}]$ indentor alignments is caused by the same wedging action of adjacent facets for this orientation. The prominent cracking for this orientation underlines the high susceptibility of (0 0 1) cracking in RDX [22].

The cracking systems associated with the Knoop impressions in the $(\bar{2}\,1\,0)$ surface of RDX appear to be operating as substitute deformation systems (i.e. in lieu of the activation of slip systems) to accommodate

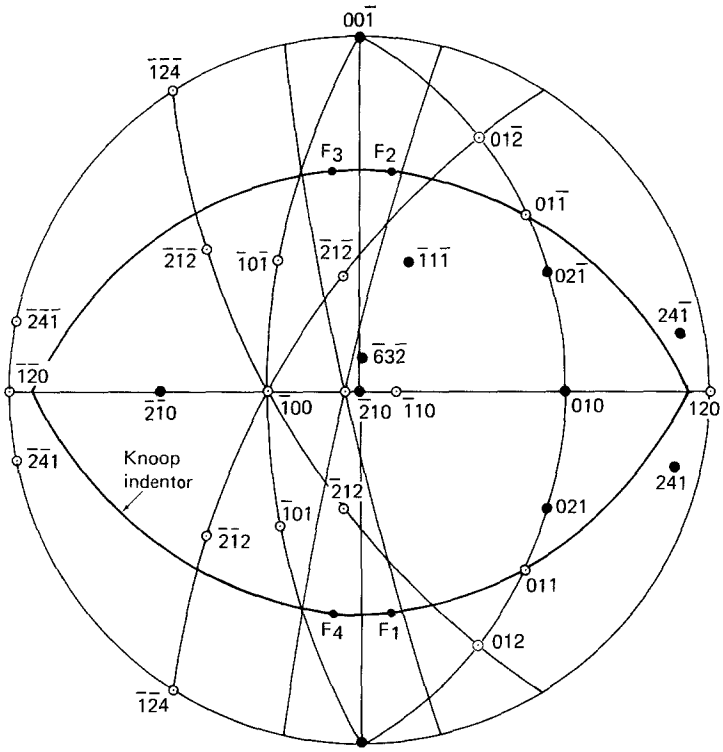


*Figure 8* ($\bar{2}\,1\,0$) stereographic projection for slip and cracking around Knoop indentations in RDX (after Armstrong and Elban [10]). (●) plane normals, (○) plane directions.

the indentor strains. Significant cracking lowered the measured hardness values. The cracking has not been associated thus far with any specific dislocation mechanism. This is important because although the Knoop hardness has been lowered, it has not been reduced to the same extent as occurs for the dislocation-controlled cracking effects observed in a parallel study of the Vickers and Meyers hardness of MgO crystals [23]. For MgO, dislocation-controlled cracking of $\{1\,1\,0\}$ planes has been associated with an indentation fracture mechanics explanation which leads to a large reduction in hardness with increase in applied load.

The hardness anisotropy for the impressions not exhibiting significant cracking is in the approximate direction given by the effective resolved shear stress (ERSS) model of Brookes *et al.* [24] for $\{0\,2\,1\}$ and $(0\,1\,0)$ $[1\,0\,0]$ slip. However, the indentations themselves have anisotropic shapes. On this basis, a different ERSS should actually apply for each facet of the indentor. For example, Figs 1a and b give clear evidence that the deformation pattern is not the same for each facet. On the left-hand side of the Knoop impression in Fig. 1a, only $(0\,2\,1)$ or $(0\,2\,\bar{1})$ slip occurred in any obvious way to accommodate the two appropriate facets. On the right-hand side of the impression, only $(0\,1\,0)$ slip and $(\bar{1}\,0\,0)$ cracking appear to have occurred. The total slip systems are insufficient to accommodate the indentor strains, hence, the suggested need of considering, in addition, the orientation dependence of cracking.

A stereographic projection description of the Knoop hardness test is given in Fig. 8 to help in understanding the crystallography involved in the hardness measurements and associated cracking behaviour for RDX. The projection is centred on the $(\bar{2}\,1\,0)$ plane surface of the crystal and contains information relating to all of the deformation systems previously identified [7, 18]. One position for the Knoop indentor is shown oriented along the $[\bar{1}\,\bar{2}\,0]$ direction. The hypothesized direction of the effective force, $F$, associated with each facet in the calculation of an ERSS is shown in the respective position contained in the plane of the indentor facet.

In addition to identifying operative slip systems in RDX from the limited information that exists, there is also the question of the role of work hardening in interpreting [25, 26] the Knoop hardness anisotropy in terms of those slip systems proposed to be available. For example, the $[\bar{1}\,0\,0]$ direction is common to the $(0\,2\,1)$, $(0\,2\,\bar{1})$ and $(0\,1\,0)$ planes (in Fig. 8), thus providing the necessary crystallographic condition for cross-slip of dislocations to occur among the planes. This observation provides a possible explanation for the lack of well-defined slip traces around the hardness impressions. This further connects with the high homologous temperature at which the room-temperature hardness tests were performed on RDX. The expectation is that cross-slip should be promoted with increasing temperature, as well as the further possibility that additional slip systems would become operative, which does not appear to be occurring here. However, care must be taken in applying the same homologous temperature considerations to molecular crystalline solids as would normally apply to metallic systems.

The highly localized strain fields surrounding the hardness impressions in the $(\bar{6}\,3\,\bar{2})$ topographic image in Fig. 7 indicate that dislocation movement in the RDX lattice is very difficult. Based on the transmission X-ray topographic observations of Halfpenny *et al.* [18], dislocation formation (generation) seems to be easy because a large variety of Burgers vectors were found for different dislocations in carefully grown RDX crystals. This compares with a variety of other crystalline materials where dislocation generation and movement are strongly coupled, and their influences on deformation properties are not easily distinguished. Despite the variety of dislocation Burgers vectors and

line vectors established for these defects in RDX, movement of the defects seems to be exceptionally difficult. Further study is being made of the possibility that the explanation is rooted in the complicated intermolecular interactions characteristic of the basic crystal structure [8]. For example, a preliminary analysis of the intermolecular shear displacements across (0 2 1) indicates that $\pm[0\,1\,\bar{2}]$ direction slip should be favourable for dislocations with a corresponding Burgers vector [27, 28].

## 6. Conclusions

1. Topographic observations of a carefully grown RDX crystal show the presence of internal strains due to the crystal growth process, thus providing evidence for the existence of substantial internal obstacles to the propagation of slip bands and cracks.

2. Extremely localized plastic deformation zones surrounding Knoop microindentations are observed by X-ray topography and are further evidence that very restricted dislocation motion occurs in the RDX lattice.

3. Individual cleavage cracking systems operate at different Knoop indentor orientations so as to help accommodate the imposed indentation strains, thereby also contributing to the measured anisotropy for the hardness measurements.

## Acknowledgements

This work was sponsored by the Office of Naval Research (ONR) under work request numbers N00014-82-WR-20129, N00014-83-WR-30046, N00014-84-WR-24086, N00014-85-WR-24103, NR 659-797, N00014-82-K-0263, NR 659-798, N00014-86-K-0286, NR 432h-021, and N000140-87-K-0175, NR 432h-803, as a cooperative effort between the Naval Surface Warfare Center (NSWC), White Oak, the University of Maryland, College Park, Maryland and Loyola College, Baltimore, Maryland. The authors thank J. R. Holden and C. W. Dickinson for use of X-ray facilities at NSWC and for helpful advice. Particular thanks are given to R. R. Bernecker for helpful discussion and constructive comments concerning the manuscript.

## References

1. M. J. KAMLET, in "Sixth Symposium (International) on Detonation", Coronado, CA, August 1976, Office of Naval Research, Department of the Navy, Arlington, Virginia, ACR-221, p.312.
2. M. J. KAMLET and H. G. ADOLPH, *Propel. Explos.* **4** (1979) 30.
3. F. P. BOWDEN and A. D. YOFFE, "Fast Reactions in Solids" (Butterworths Scientific, London, 1958).
4. C. S. COFFEY and R. W. ARMSTRONG, in "Shock Waves and High-Strain-Rate Phenomena in Metals", edited by M. A. Meyers and L. E. Murr (Plenum, New York, 1981) p. 313.
5. R. W. ARMSTRONG, C. S. COFFEY and W. L. ELBAN, *Acta Metall.* **30** (1982) 2111.
6. *Idem*, in "Advances in Chemical Reaction Dynamics", edited by P. M. Rentzepis and C. Capellos (Reidel, Boston, 1986) p. 469.
7. W. L. ELBAN and R. W. ARMSTRONG, in "Proceedings of the Seventh Symposium (International) on Detonation", Annapolis, Md, 16–19 June 1981, Naval Surface Weapons Center, Silver Spring, Maryland, 1982, NSWC MP 82-334, p. 976.
8. W. L. ELBAN, J. C. HOFFSOMMER and R. W. ARMSTRONG, *J. Mater. Sci.* **19** (1984) 552.
9. W. CONNICK and F. G. J. MAY, *J. Crystal Growth* **5** (1969) 65.
10. R. W. ARMSTRONG and W. L. ELBAN, in "Microindentation Techniques in Materials Science and Engineering", ASTM STP 889, edited by P. J. Blau and B. R. Lawn (American Society for Testing and Materials, Philadelphia, Pennsylvania, 1986) p. 109.
11. P. J. HALFPENNY, K. J. ROBERTS and J. N. SHERWOOD, *J. Mater. Sci.* **19** (1984) 1629.
12. R. W. ARMSTRONG and C. CM. WU, in "Microstructural Analysis: Tools and Techniques", edited by J. L. McCall and W. M. Mueller (Plenum, New York and London, 1973) p. 169.
13. B. K. TANNER, "X-ray Diffraction Topography" (Pergamon, Oxford, 1976).
14. R. W. ARMSTRONG, in "Characterization of Crystal Growth Defects by X-Ray Methods", edited by B. K. Tanner and D. K. Bowen (Plenum, New York, London, 1980) p. 349.
15. R. W. ARMSTRONG, in "Applications of X-ray Topographic Methods to Materials Science", edited by S. Weissman, F. Balibar and J. F. Petroff (Plenum, New York, 1984) p. 33.
16. H. KLAPPER, in "Characterization of Crystal Growth Defects by X-ray Methods", edited by B. K. Tanner and D. K. Bowen (Plenum, New York, London, 1973) p. 133.
17. I. T. McDERMOTT and P. P. PHAKEY, *Phys. Status Solidi (a)* **8** (1971) 505.
18. P. J. HALFPENNY, K. J. ROBERTS and J. N. SHERWOOD, *Phil. Mag.* **A53** (1986) 531.
19. M. F. ASHBY and L. M. BROWN *ibid.* **8** (1963) 1083.
20. J. JUNG and M. LEFELD-SOSNOWSKA, *ibid.* **A50** (1984) 233.
21. B. ROESSLER and R. W. ARMSTRONG, *Adv. X-ray Anal.* **12** (1969) 139.
22. J. T. HAGAN and M. M. CHAUDHRI, *J. Mater. Sci.* **12** (1977) 1055.
23. K. C. YOO, R. G. ROSEMEIER, W. L. ELBAN and R. W. ARMSTRONG, *J. Mater. Sci. Lett.* **3** (1984) 560.
24. C. A. BROOKES, J. B. O'NEILL and B. A. W. REDFERN, *Proc. R. Soc. Lond.* **A322** (1971) 73.
25. R. W. ARMSTRONG and A. C. RAGHURAM, in "The Science of Hardness Testing and Its Research Applications", edited by J. H. Westbrook and H. Conrad (American Society for Metals, Metals Park, Ohio, 1973) p.174.
26. R. W. ARMSTRONG, and C. CM. WU, *J. Amer. Ceram. Soc.* **61** (1978) 102.
27. R. W. ARMSTRONG and W. L. ELBAN, in "Energetic Materials Initiation Fundamentals Workshop", Los Alamos National Laboratory, 14-17 October 1986 (Chemical Propulsion Information Agency, 1987) Publ. 475, p. 177.
28. T. J. BODINE, D. R. HUGHES, H. L. AMMON and R. W. ARMSTRONG, unpublished research.

*Received 2 February*
*and accepted 13 June 1988*